SUPPLEMENTARY INFORMATION

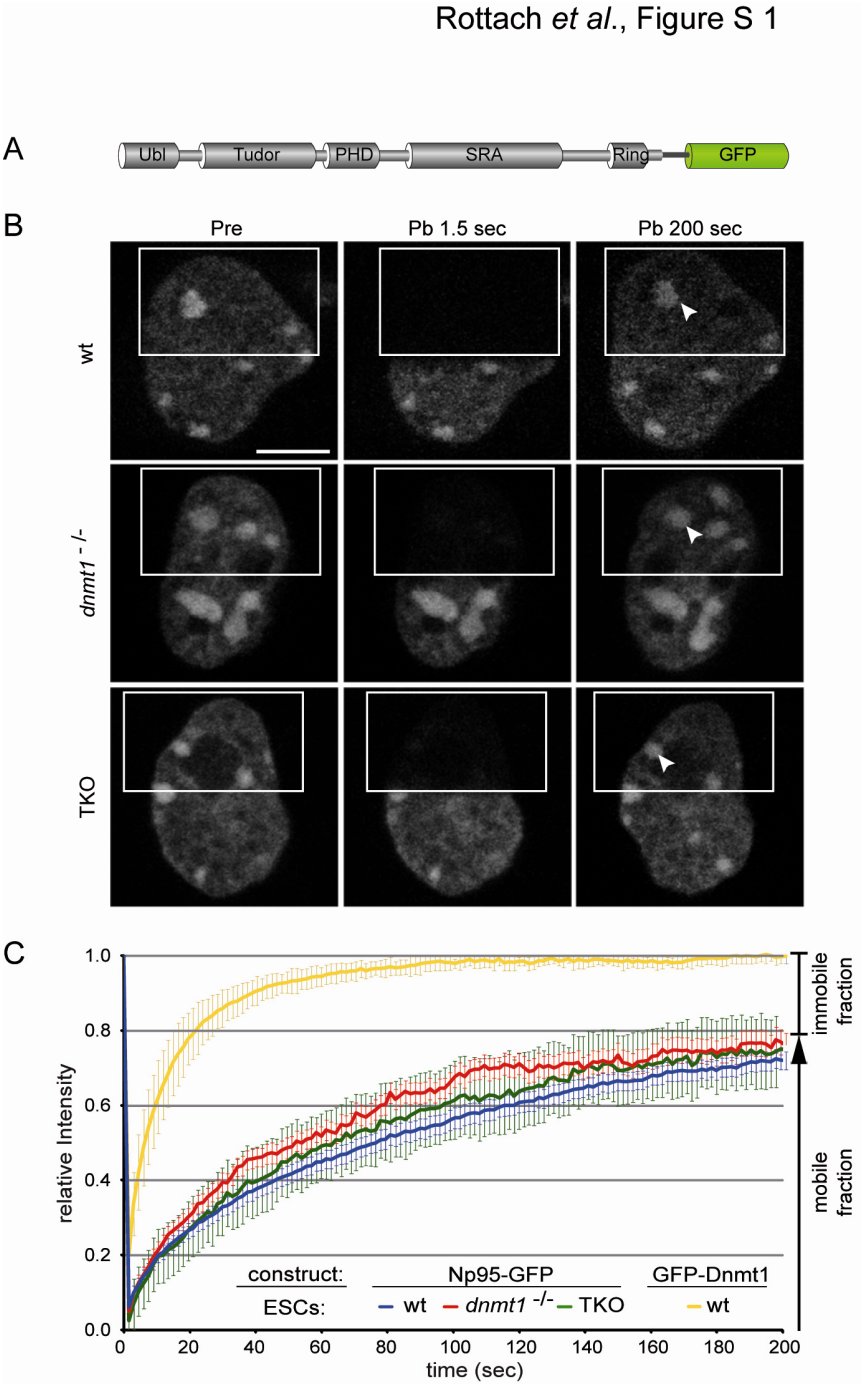

Supplementary Figure 1. Nuclear localization, FRAP kinetics and DNA binding specificity for an Np95 construct C-terminally fused to GFP (Np95-GFP, respectively). (**A**) Schematic drawing of Np95-GFP. Abbreviations are as in Fig. 1. (**B**) Representative images from FRAP experiments for Np95-GFP transiently expressed in wt, *dnmt1*$^{-/-}$ and TKO J1 ESCs as indicated on the left. Images show confocal mid-sections of nuclei before (Pre) and at the indicated time points after bleaching (Pb) half of the nucleus. Bleached areas are outlined. Arrowheads mark pericentric heterochromatin. Bars, 5 µm. **(C**) FRAP kinetics of Np95-GFP in J1 ESCs with different genetic backgrounds as shown in B and Fig. 1C. Kinetics of GFP-Dnmt1 is shown for comparison. Mobile and immobile fractions are indicated on the right. Values represent mean ± SEM. Note that the kinetics are similar to those shown for GFP-Np95 in Fig. 1C and that there is no significant difference in cells with different genetic backgrounds.

Rottach *et al.*, Figure S 2

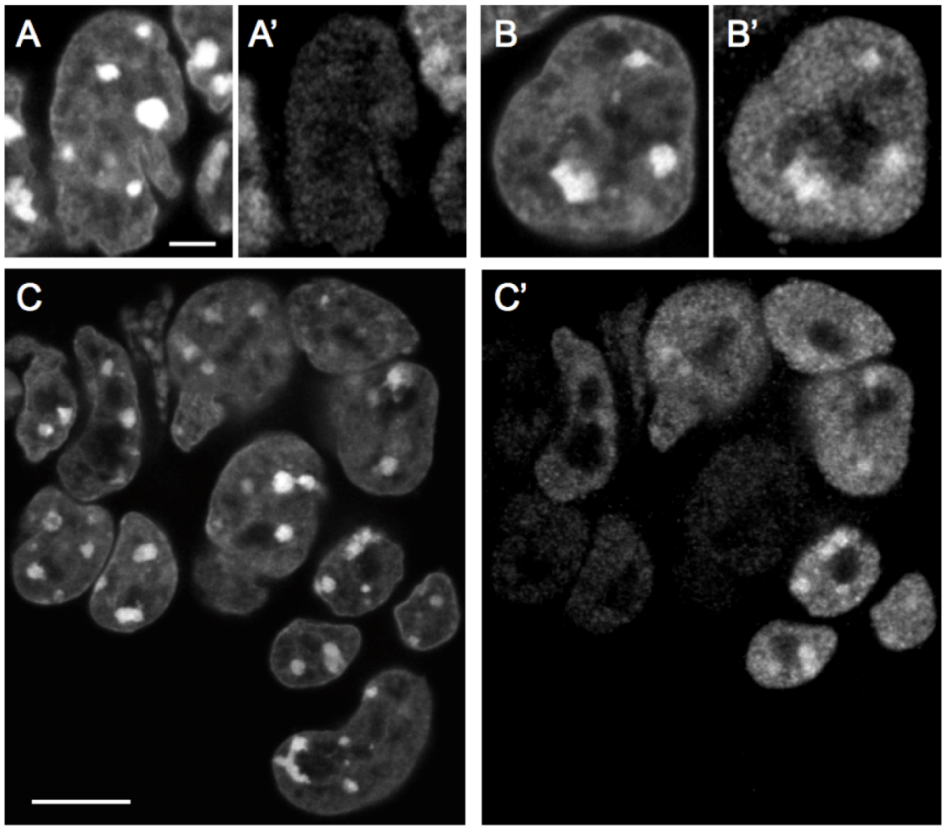

Supplementary Figure 2. Variable expression levels and localization of Np95 in TKO cells. TKO cells were stained with DAPI (A, B and C) and an anti-Np95 antibody (A', B' and C'). A-A' and B-B' show examples of cells with very low and high Np95 levels, respectively. In B' accumulation of endogenous Np95 at chromocenters is evident. C and C' show a field containing cells with very different Np95 levels and degrees of Np95 accumulation at chromocenters. Scale bars are 3 μm (A-B') and 10 μm (C and C').

Rottach *et al.*, Figure S 3

A

Oligo name	DNA sequence
CG-up	5'- CTCAACAACTAACTACCATCCGGACCAGAAGAGTCATCATGG -3'
MG-up	5'- CTCAACAACTAACTACCATCMGGACCAGAAGAGTCATCATGG -3'
3CG-up	5'-CTCAACAACTAACTACCATCCGGACCTCATCCGGACCTCATCCGGACCAGAAGAGTCATCATGG -3'
Fill-In-550	5'- ATTO550-CCATGATGACTCTTCTGGTC -3'
Fill-In-647N	5'- ATTO647N-CCATGATGACTCTTCTGGTC -3'

B

Substrate	CpG site	Label	Oligo I	Oligo II	dCTP reaction
UMB-550	unmethylated	550	CG-up	Fill-In-550	dCTP
UMB-647N		647N		Fill-In-647N	
HMB-550	hemimethylated	550	MG-up	Fill-In-550	dCTP
HMB-647N		647N		Fill-In-647N	
UMB-3CG-550	unmethylated	550	3CG-up	Fill-In-550	dCTP
UMB-3CG-647N		647N		Fill-In-647N	
HMB-3CG-550	hemimethylated	550	3CG-up	Fill-In-550	5methyl dCTP
HMB-3CG-647N		647N		Fill-In-647N	

Supplementary Figure 3. Oligo design for the *in vitro* DNA binding assay (**A**) DNA oligonucleotides used for the preparation of double stranded probes for *in vitro* DNA binding assays. M: 5-methyl-cytosine. (**B**) Description of double stranded probes used for *in vitro* DNA binding assays. Name, status of the central CpG site, fluorescent label, as well as DNA oligonucleotides and nature of the dCTP used in the primer extension reaction are specified. By using a control set of two probes with identical sequence but different fluorescent labels we observed effects due to probe preparation and/or unspecific binding of ATTO dyes (data not shown). The values obtained from the control set were used to normalize every probe / protein pair.

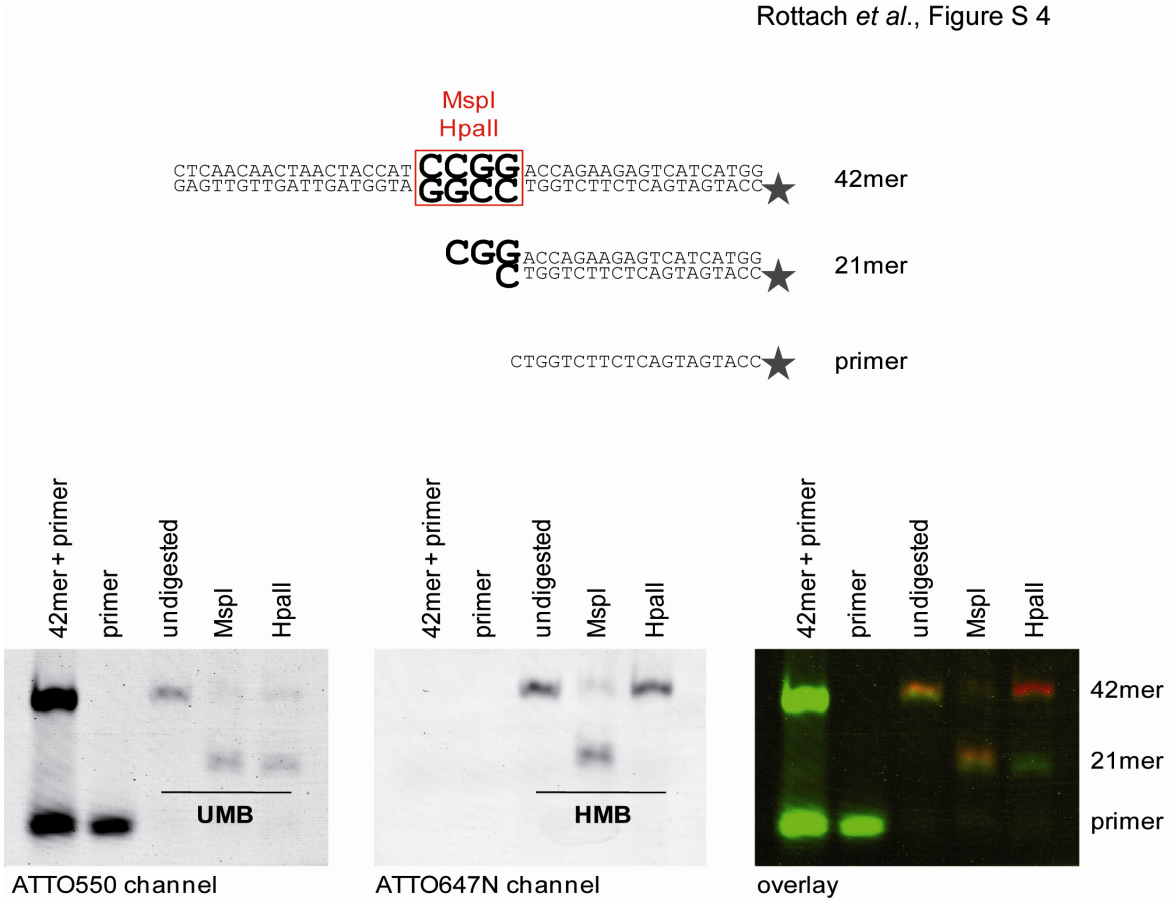

Supplementary Figure 4. Quality control of un- and hemi-methylated DNA substrates

Unmethylated and hemimethylated DNA substrates (UMB550 and HMB647N, respectively) were digested with MspI or HpaII and analyzed by 15 % non-denaturing PAGE for CG methylation. DNA substrates were detected via their fluorescent ATTO label using the Typhoon Trio scanner. Note that the unmethylated DNA substrate is digested by both MspI and HpaII, whereas the hemimethylated substrate is cut by MspI, but not by the methylation sensitive HpaII. Sequences of the double stranded probes before (42mer) and after cut (21mer) as well as the unextended primer are displayed above. Enzyme recognition motifs are boxed and asterisks represent fluorescent ATTO label.

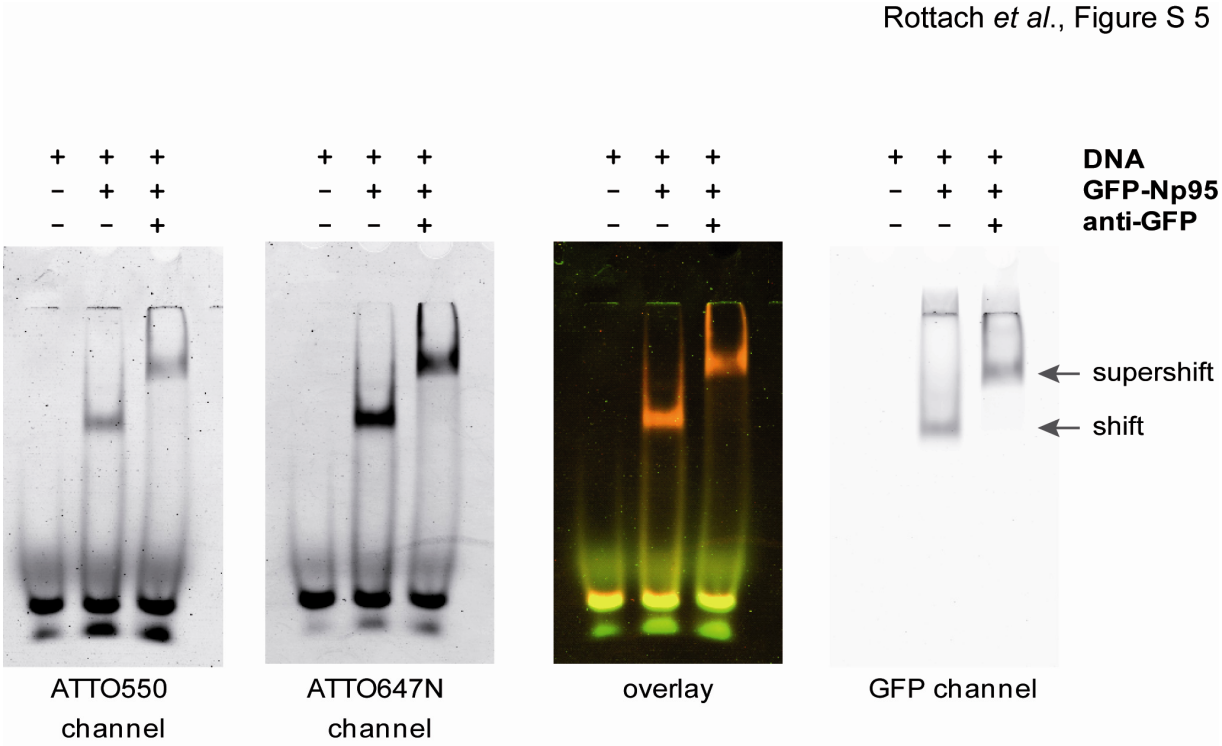

Supplementary Figure 5. Electrophoretic mobility shift and supershift assays with GFP-Np95. Un- and hemimethylated DNA substrates (1 pmol UMB550 and HMB647N, respectively) were incubated with 0.6 pmol purified GFP-Np95 and 0.4 pmol GFP-antibody. Samples were subjected to a 3.5 % non-denaturing PAGE and analyzed by the Typhoon Trio scanner to detect ATTO550 (unmethylated substrate), ATTO647N (hemimethylated substrate) and green fluorescence (GFP). Note that the DNA:GFP-Np95:GFP-antibody complex is shifting higher than the DNA:GFP-Np95 complex (arrows).

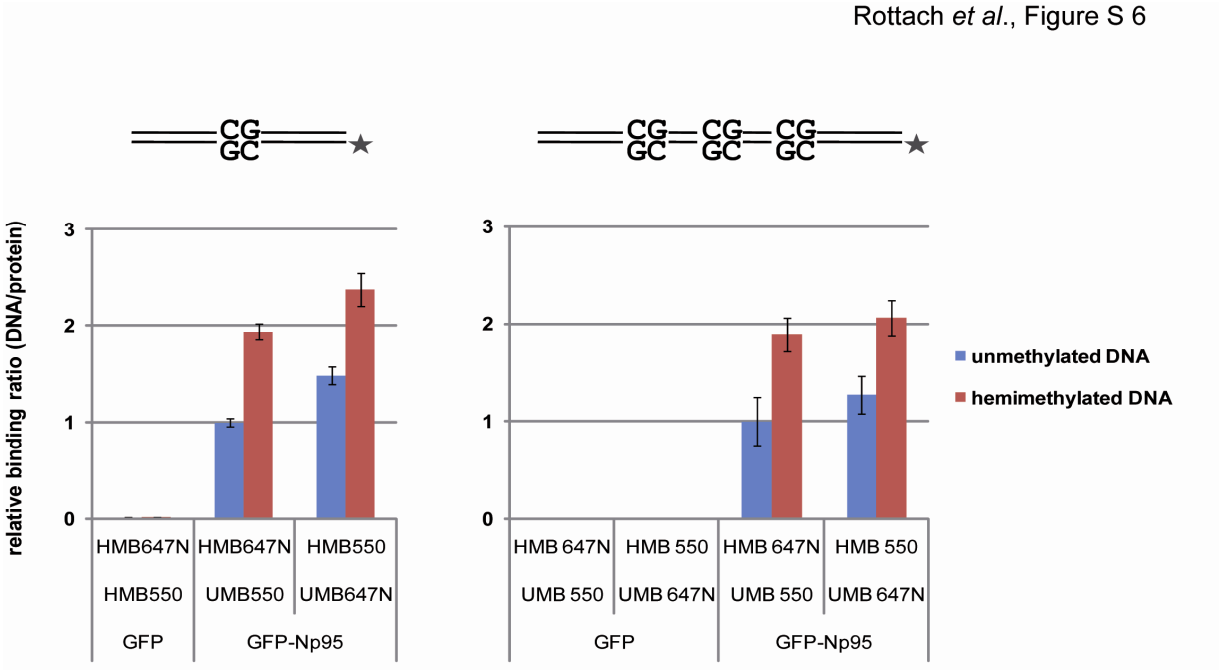

Supplementary Figure 6. DNA binding specificity of GFP-Np95

The sequence specific DNA binding activity of Np95 was tested with an *in vitro* binding assays using GFP-Np95 with un- and hemimethylated substrates in direct competition. The DNA substrates included either one (left) or three (right) CG sites. Note that regardless of the attached fluorescent label (indicated by asterisks) and number of CG sites the hemimethylated DNA substrates are preferentially bound (1.6- to 1.9-fold). Shown are the means ± SEM from two (left) or four (right) independent experiments.

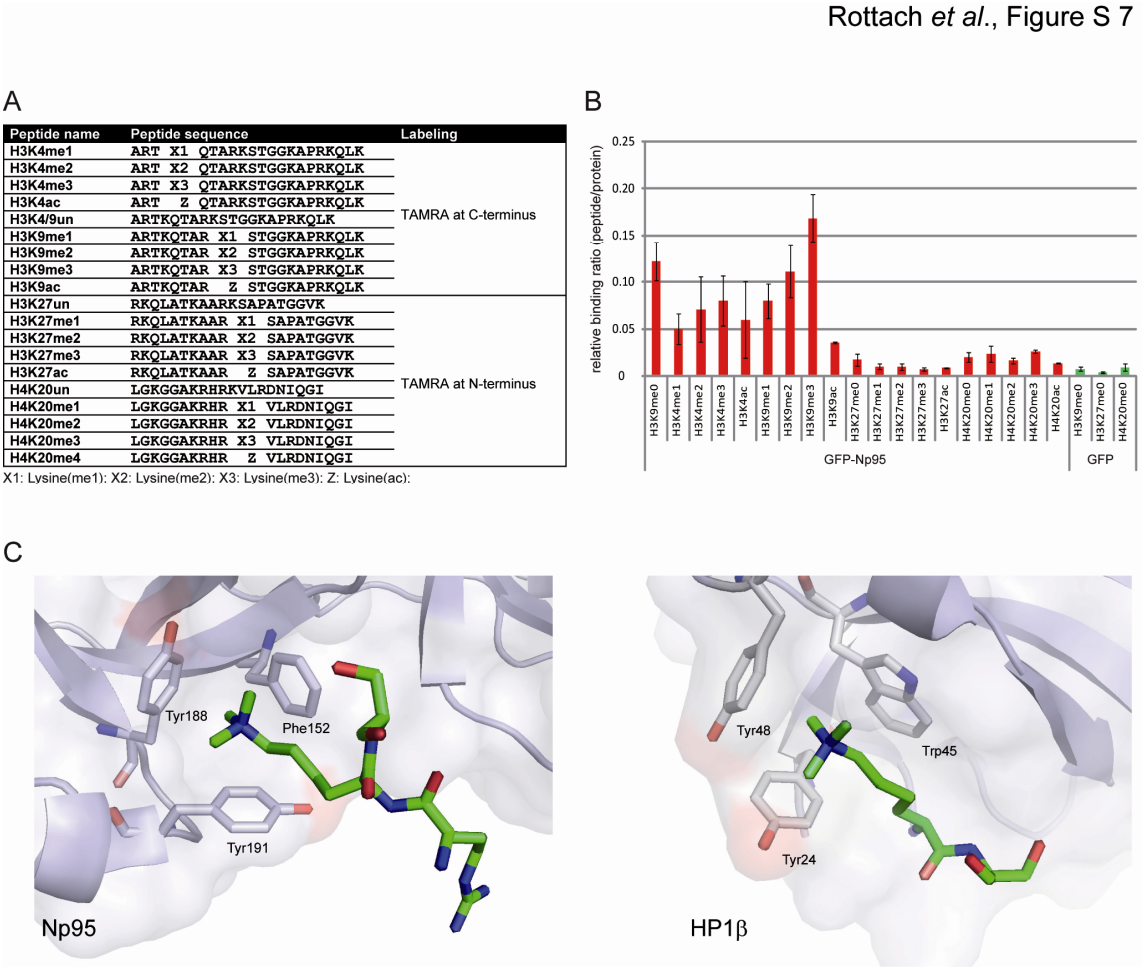

Peptide name	Peptide sequence	Labeling
H3K4me1	ART X1 QTARKSTGGKAPRKQLK	TAMRA at C-terminus
H3K4me2	ART X2 QTARKSTGGKAPRKQLK	
H3K4me3	ART X3 QTARKSTGGKAPRKQLK	
H3K4ac	ART Z QTARKSTGGKAPRKQLK	
H3K4/9un	ARTKQTARKSTGGKAPRKQLK	
H3K9me1	ARTKQTAR X1 STGGKAPRKQLK	
H3K9me2	ARTKQTAR X2 STGGKAPRKQLK	
H3K9me3	ARTKQTAR X3 STGGKAPRKQLK	
H3K9ac	ARTKQTAR Z STGGKAPRKQLK	
H3K27un	RKQLATKAARKSAPATGGVK	TAMRA at N-terminus
H3K27me1	RKQLATKAAR X1 SAPATGGVK	
H3K27me2	RKQLATKAAR X2 SAPATGGVK	
H3K27me3	RKQLATKAAR X3 SAPATGGVK	
H3K27ac	RKQLATKAAR Z SAPATGGVK	
H4K20un	LGKGGAKRHRKVLRDNIQGI	
H4K20me1	LGKGGAKRHR X1 VLRDNIQGI	
H4K20me2	LGKGGAKRHR X2 VLRDNIQGI	
H4K20me3	LGKGGAKRHR X3 VLRDNIQGI	
H4K20me4	LGKGGAKRHR Z VLRDNIQGI	

X1: Lysine(me1): X2: Lysine(me2): X3: Lysine(me3): Z: Lysine(ac):

Supplementary Figure 7. Histone tail binding of Np95 and HP1ß (**A**) Amino acid sequences of TAMRA-labeled histone tail peptides used for the peptide binding assay. (**B**) Histone H3 and H4-tail binding specificity of GFP-Np95 *in vitro*. Ratios of bound TAMRA-labeled peptide over bound GFP fusion were determined and normalized to the ratio of H3K4/9un peptide over GFP-Np95. GFP was used as negative control. Shown are means ± SEM from six independent experiments. (**C**) Structural comparison of the H3K9me3-binding aromatic cages formed by the tandem Tudor domain of Np95 (left) and the chromodomain of HP1ß (right, PDB 1kne). In these structures, only Arg8-Lys9-Ser10 and Lys9-Ser10 from histone H3 are resolved peptides, respectively (green stick models). The image was generated with PyMOL (1).

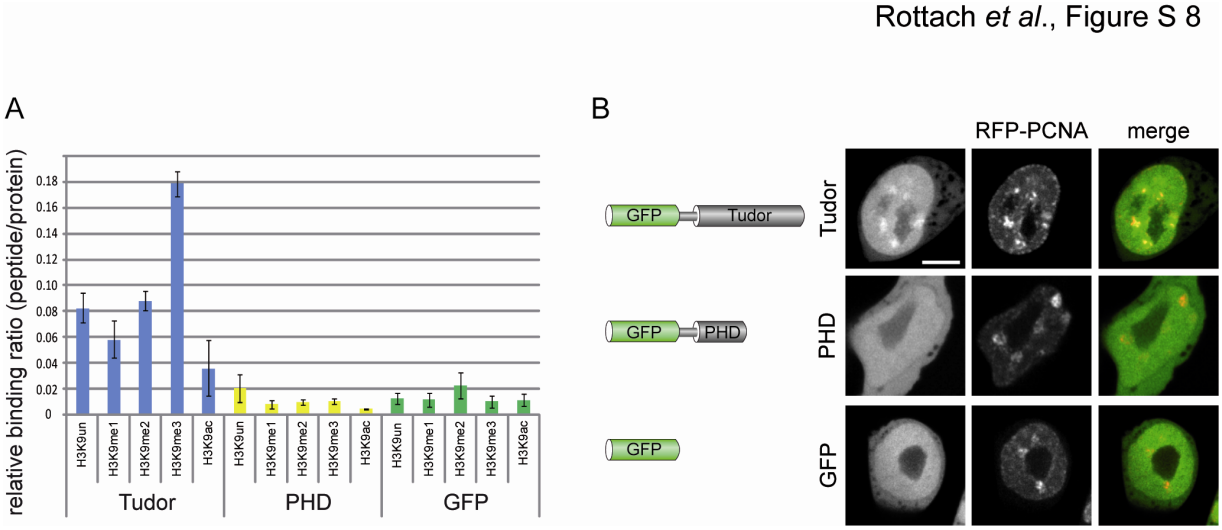

Supplementary Figure 8. Histone tail binding and subcellular distribution of PHD and Tudor domain of Np95 (**A**) Histone H3 N-terminal tail binding specificity of GFP-Tudor, GFP-PHD and GFP *in vitro*. Shown are fluorescence intensity ratios of bound probe / bound GFP fusion. GFP was used as negative control. Shown are means ± SEM from four to six independent experiments. Only the tandem Tudor domain shows preferential binding of H3K9 trimethylated histone tails. (**B**) Schematic representation of the analyzed Np95 constructs. All constructs were N-terminal GFP fusions (left panel). Confocal mid sections of living *np95*$^{-/-}$ ESCs transiently expressing the indicated Np95 fusion constructs and RFP-PCNA as S phase marker (left and mid panels). Merged images are displayed on the right. Bars, 5 µm. Only the GFP-Tudor fusion protein showed slight enrichment at pericentric heterochromatin.

References:

1. DeLano, W.L. (2002) *The PyMOL User's Manual*.